The Asphaltenes

Oliver C. Mullins

Schlumberger-Doll Research, Cambridge, Massachusetts 02139; email: Mullins1@slb.com

Annu. Rev. Anal. Chem. 2011. 4:393–418

The *Annual Review of Analytical Chemistry* is online at anchem.annualreviews.org

This article's doi:
10.1146/annurev-anchem-061010-113849

1936-1327/11/0719-0393$20.00

Keywords

island molecular architecture, nanoaggregate, nanoaggregate cluster, molecular weight, molecular architecture, modified Yen model, Yen-Mullins model

Abstract

Asphaltenes, the most aromatic of the heaviest components of crude oil, are critical to all aspects of petroleum utilization, including reservoir characterization, production, transportation, refining, upgrading, paving, and coating materials. The asphaltenes, which are solid, have or impart crucial and often deleterious attributes in fluids such as high viscosity, emulsion stability, low distillate yields, and inopportune phase separation. Nevertheless, fundamental uncertainties had precluded a first-principles approach to asphaltenes until now. Recently, asphaltene science has undergone a renaissance; many basic molecular and nanocolloidal properties have been resolved and codified in the modified Yen model (also known as the Yen-Mullins model), thereby enabling predictive asphaltene science. Advances in analytical chemistry, especially mass spectrometry, enable the identification of tens of thousands of distinct chemical species in crude oils and asphaltenes. These and other powerful advances in asphaltene science fall under the banner of petroleomics, which incorporates predictive petroleum science and provides a framework for future developments.

1. INTRODUCTION

One learns in elementary school science that matter is composed of solids, liquids, and gases. Crude oils contain all three phases. The gas and liquid components of crude oils are amenable to various chemical analyses and treatment by variations of the van der Waals equation. However, until recently, the asphaltenes—crude oil solids (1–3) that are defined operationally (e.g., toluene soluble, *n*-heptane insoluble)—had not been chemically understood, which precluded any first-principles treatment. Virtually all asphaltene chemical properties, excepting elemental composition, had been the subject of debate; their molecular weight had been estimated at values spanning six orders of magnitude (4). Nevertheless, an understanding of asphaltenes is essential because they have a significant impact on many physical and chemical properties of crude oils and related systems.

Recent, diverse analyses to characterize asphaltenes have led to the development of a single, relatively simple framework—the modified Yen Model (5). Advances in analytical chemistry have enabled a much more comprehensive chemical analysis of all the components of crude oil. Fourier transform ion cyclotron resonance mass spectrometry (FT-ICR MS) has revolutionized petroleum analysis by providing explicit elemental composition for up to 100,000 components of crude oil (6). This advance portends predictive petroleum science, or petroleomics (1, 6), much as the ability to read the human genome has enabled genomics. New analytical methods applied to the nonasphaltene components (the maltenes) of crude oil, such as two-dimensional gas chromatography, also obtain chemical specificity, as opposed to "lumped" or pseudocomponents (7).

Geochemical analyses of hydrocarbon fluids can be highly informative, especially about the geologic processes that shape petroleum systems (8). The broader context of the physical and chemical attributes of petroleum, especially involving asphaltenes, is becoming increasingly essential for optimal resource utilization (1). The modified Yen model and new theoretical methods of asphaltenes are being combined with a new technology known as downhole fluid analysis (DFA) (9), which delineates the spatial distribution of reservoir fluids (9) to enhance oil reservoir characterization (10). Asphaltene surface science has advanced through many studies framed within the modified Yen model (5). Deleterious phase-separated asphaltenes in production facilities are being mitigated within a petroleomics perspective, thereby improving flow assurance (11). Stabilization of petroleum emulsions is becoming increasingly understood at the molecular level (12, 13). The challenge of molecular management of refining mandates proper molecular characterization of all the components of crude oil (14). Thermodynamic treatments of heavy ends illustrate that four hydrocarbon phases—a gas, two liquids, and a solid—can exist simultaneously (15). Asphaltenes are concentrated in many reservoirs due to the biodegradation of reservoir crude oils (16). In an environmental context, asphaltenes and their recalcitrant derivatives arise in significant quantities in the world's oceans and come from many sources, including man-made spills and natural sources such as asphaltene volcanoes on the seafloor (17).

In this review, I discuss the tremendous advances in molecular and colloidal asphaltene science, focusing on the modified Yen model with particular emphasis on asphaltene molecular weight and architecture. Diverse asphaltene studies that address single topics provide robust conclusions. The connection between basic science and application is central to this review. I outline theoretical developments in asphaltene phase behavior and asphaltene gradients in oil reservoirs, present simple foundations for asphaltene surface science, and discuss viscosity versus asphaltene content and temperature within a simple context. The dramatic developments in asphaltene science are rapidly improving efficiency in petroleum resource utilization.

Table 1 Issues in asphaltene science that have been resolved over the past 10 years

Scientific issue	Range of reported values (as of ~1998)	Values (as of 2010)	Width of distribution (as of 2010)
Asphaltene molecular weight	Less than 1,000 Da to 1,000,000,000 Da	750 Da	400–1,000 FWHM
Number of PAHs in an asphaltene molecule	1 to 20	1 dominates	Small mass fraction with 0, 2, 3, etc., ring systems
Number of fused rings per PAH in asphaltene	2 to 20	7	4–10
Number of PAH stacks in asphaltene nanoaggregate	Unknown	1	—
Aggregation number of nanoaggregates	10–100	<10	4–10
Critical nanoaggregate concentration of asphaltenes	50 mg liter^{-1} to 5 g liter^{-1}	100 mg liter^{-1}	50–150 mg liter^{-1}
Concentration of cluster formation	Unknown	~3 g liter^{-1}	2–5 g liter^{-1}
Size of cluster	Unknown	6 nm for small clusters	Probably larger clusters also depending on temperature, concentration
Role of resins in asphaltene nanoaggregate	None to necessary	~15% of crude oil nanoaggregates are resins; resins are not surfactants	Depends on definitions
Relation of nanoaggregate to cluster	Unknown	Clusters consist of nanoaggregates	—
Relation of nanoaggregates in toluene to those in crude oil	Unknown	Very similar in size and composition	—

Abbreviations: FWHM, full width at half maximum; PAH, polycyclic aromatic hydrocarbon.

2. THE MODIFIED YEN MODEL

2.1. The Yen Model

In 1967, Professor Teh Fu Yen[1] and coworkers (18) proposed a model to account for the structural elements of asphaltenes. This model, now known as the Yen model, specifically accounted for different chemical moieties in asphaltenes such as polycyclic aromatic hydrocarbons (PAHs), PAH stacks, alkane, petroporphyrins, and the like.

Since the Yen model was first proposed, it has helped to guide research, particularly for bulk measurements on phase-separated asphaltenes. Nevertheless, the Yen model has significant limitations. When it was first proposed, there was little consensus on important asphaltene molecular and colloidal properties.

2.2. Resolution of Asphaltene Molecular and Colloidal Properties

Table 1 lists previously unresolved issues, often involving estimates spanning orders of magnitude, that had long plagued the field of asphaltene science. Fortunately, the past decade has seen huge advances in this field.

[1]Professor Teh Fu Yen recently passed away. This giant in the field of asphaltene science will be missed.

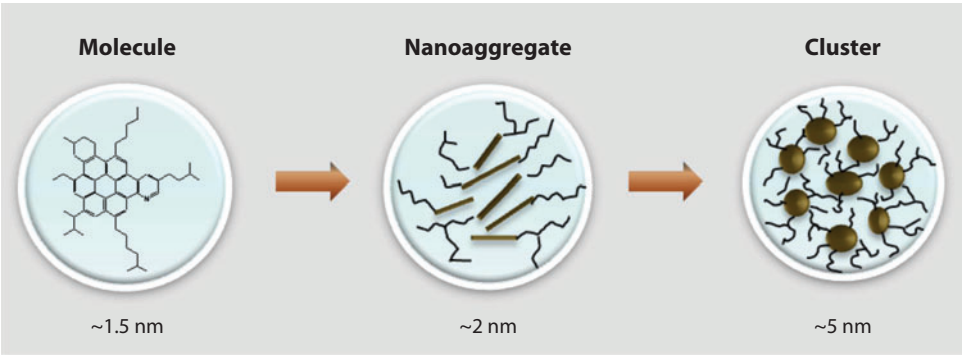

Figure 1

The modified Yen model (or the Yen-Mullins model). (*Left*) The predominant asphaltene molecular architecture contains a single, moderately large polycyclic aromatic hydrocarbon (PAH) with peripheral alkanes. (*Center*) Asphaltene molecules form nanoaggregates with aggregation numbers of approximately six, with a single disordered PAH stack. (*Right*) Asphaltene nanoaggregates can form clusters with aggregation numbers of approximately eight.

2.3. The Modified Yen Model

Recent advances in asphaltene science (**Table 1**) have been codified in the modified Yen model (**Figure 1**) (5). The modified Yen model (also known as the Yen-Mullins Model) specifies the dominant molecular and colloidal structure of asphaltenes.

3. MOLECULAR WEIGHT AND MOLECULAR ARCHITECTURE

Previously, there were many conflicting values of the molecular weight of asphaltenes obtained from weight from MS (4, 5, 19). In addition, it was unknown whether asphaltene molecules contain predominantly one PAH (the island architecture) or many cross-linked PAHs (the archipelago architecture) (20). Molecular diffusion measurements, especially from time-resolved fluorescence depolarization (TRFD), helped to resolve these molecular properties of asphaltenes (21–26). In TRFD, a polarized excitation laser beam excites and polarizes asphaltene PAHs of individual molecules in a dilute toluene solution. Fluorescence lifetimes can be measured in nanoseconds (27, 28); the immediate fluorescence is highly polarized. With time, the (excited) molecules undergo rotational diffusion, causing increasing depolarization of the ensemble. For a sphere, the correlation time τ_R is related to molecular size; $\tau_R = 6\pi\eta V/\mathrm{k}T$, where η is viscosity, V is molecular volume, k is Boltzmann's constant, and T is temperature. TRFD data (**Figure 2**) show that asphaltene molecules are characterized by relatively small correlation times; comparison with model compounds yields a molecular weight of 750 Da, with a full width at half maximum (FWHM) of 500 to 1,000 (21–26).

Moreover, asphaltene molecules exhibit a 10-fold variation in rotation rate versus the emission wavelength of the asphaltene fluorophores (21–26). Small, blue-emitting fluorophores of asphaltenes are not cross-linked to large, red-emitting fluorophores, which gives rise to the island molecular architecture (one PAH per molecule) and represents a radical departure from all previous thinking. **Figure 3** depicts proposed asphaltene molecules.

Fluorescence correlation spectroscopy (FCS) studies have been performed on asphaltenes (29–31). Ultradilute solutions of asphaltenes ($\sim 10^{-8}$ M) preclude any molecular aggregation. Confocal microscopy used for excitation and detection investigates 1 μm^3 of solution. As fluorophores

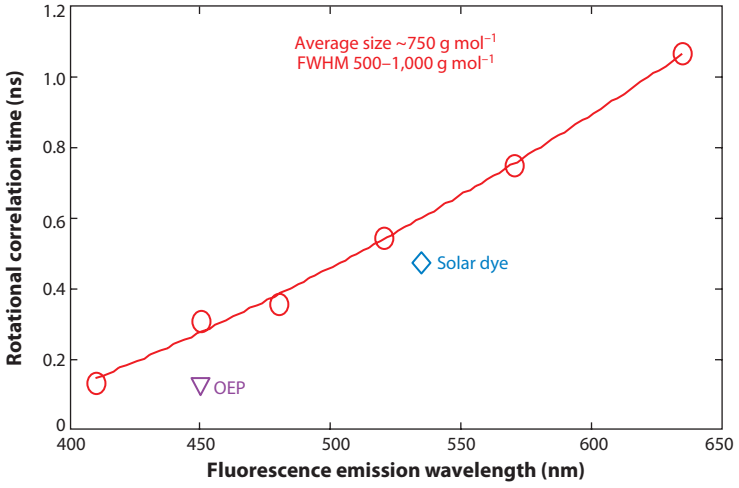

Figure 2

Time-resolved fluorescence depolarization gives the rotational correlation times of asphaltenes and model compounds [solar dye and octaethyl porphyrin (OEP)]; asphaltenes are small (~750-Da) molecules with rapid diffusion. Small, blue-emitting asphaltene fluorophores rotate much faster than large red-emitting fluorophores. These fluorophores are not cross-linked; therefore, there is one PAH per asphaltene molecule (21–26).

diffuse into and out of the confocal volume, the fluorescence signal correspondingly increases and decreases. The time decay of the autocorrelation function gives the rate of translational diffusion. Basic agreement between FCS and TRFD for petroleum- and coal-derived asphaltenes indicates that asphaltenes do not have significant internal rotational relaxation (29–31).

Two other translational diffusion measurements have been applied to asphaltenes. Nuclear magnetic resonance (NMR) translational diffusion constants are comparable to those obtained from FCS (32). These experiments rely on molecules that contain hydrogen. In addition, Taylor dispersion (TD) measurements obtain asphaltene molecular diffusion constants (33) by determining spreading rates in laminar flow using optical absorption. The TD study reports that "the [TD] results are consistent with the results obtained by Groenzin and Mullins" (33, p. 1,406). All these diffusion studies apply to asphaltene molecules that (*a*) fluoresce, (*b*) are colored, or (*c*) possess hydrogen, thereby encompassing all the constituents of asphaltenes.

4. MASS SPECTROMETRY

MS applied to asphaltenes has three main concerns: fragmentation, gas-phase aggregation, and the inability to volatilize the heaviest asphaltene fraction. These concerns nominally explain conflicting reports. An early field ionization study obtained a value of 1 kD for the most probable asphaltene molecular weight (34). Laser desorption/ionization MS (LDI) has become popular; in this approach, the sample is placed on a metal surface that is introduced into a vacuum chamber. A single laser pulse both desorbs and ionizes the sample, creating a plasma. Time of flight of ions in an electric field determines the mass-to-charge ratio. Some investigators obtained ~400 Da (35), and others obtained ~10,000 Da (36). Excessive gas-phase aggregation in LDI leads to incorrect, excessive mass measurements (37–39). Such aggregation depends on a plasma in high–laser power, high–surface concentration asphaltenes, as well as on fast collection of gas-phase ions following

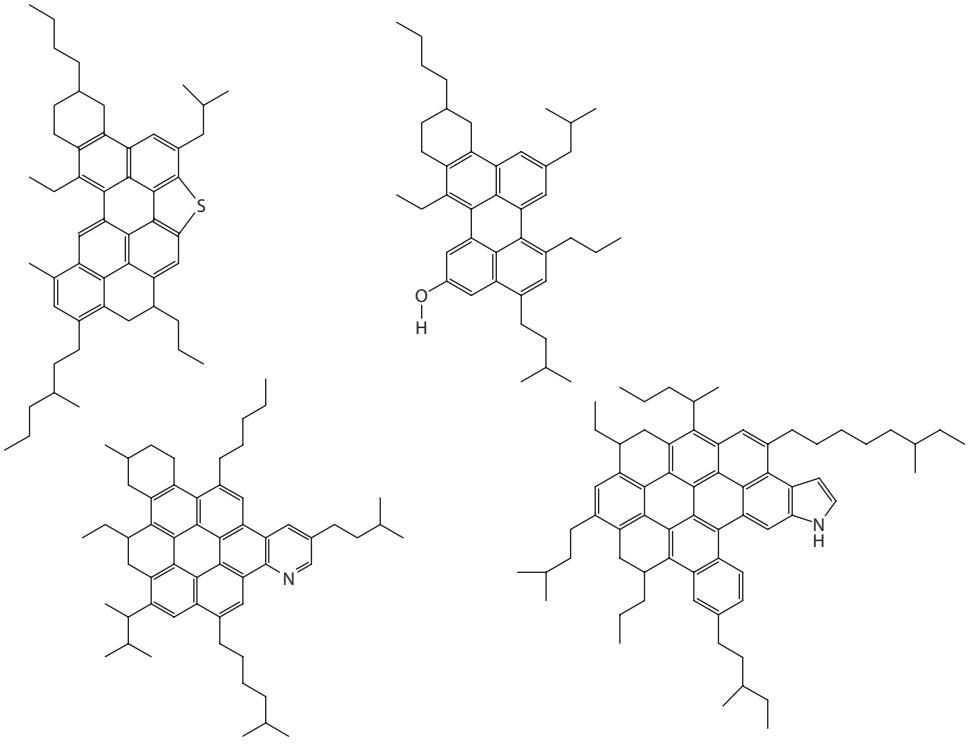

Figure 3

Typical asphaltene molecular architecture. Molecules are roughly 750 Da, and there is a single fused aromatic ring system per molecule (island molecular architecture).

laser firing. In LDI, coronene can readily aggregate to hexamers (**Figure 4**) (39). With minimized artifacts, LDI yields asphaltene masses of ~600 amu—a result similar to those obtained from molecular diffusion (37–39).

Novel two-step laser MS (L^2MS) utilizes both an infrared (IR) laser to desorb the sample and an ultraviolet (UV) laser to ionize the neutral, unaggregated plume (40–41a). The L^2MS method yields asphaltene masses of ~600 Da, independent of IR laser power, UV laser power, the surface concentration of asphaltenes, or the collection time of the ions.

Ultrahigh-resolution MS utilizing electrospray ionization (ESI) and atmospheric pressure photoionization (APPI), combined with FT-ICR MS, has been applied to the study of crude oils and asphaltenes (5, 42–45); the most probable molecular weight of asphaltenes is 750 Da (45). Laser-induced acoustic desorption, electron impact (LIAD EI) MS obtained a value of 750 Da with a width of 500 to 1,000 Da (46, 47). APPI (48) and APCI (atmospheric pressure chemical ionization) (48, 49) also obtain comparable asphaltene molecular weights. Field desorption MS obtained similar but slightly higher masses for asphaltenes (50). A good working value of asphaltene molecular weight is 750 Da, with 500–1,000 Da FWHM.

5. MOLECULAR ARCHITECTURE

TRFD asphaltene data show that blue-fluorescing chromophores rotate 10 times faster than do red-fluorescing chromophores (**Figure 2**); this finding demonstrates that the fluorophores are

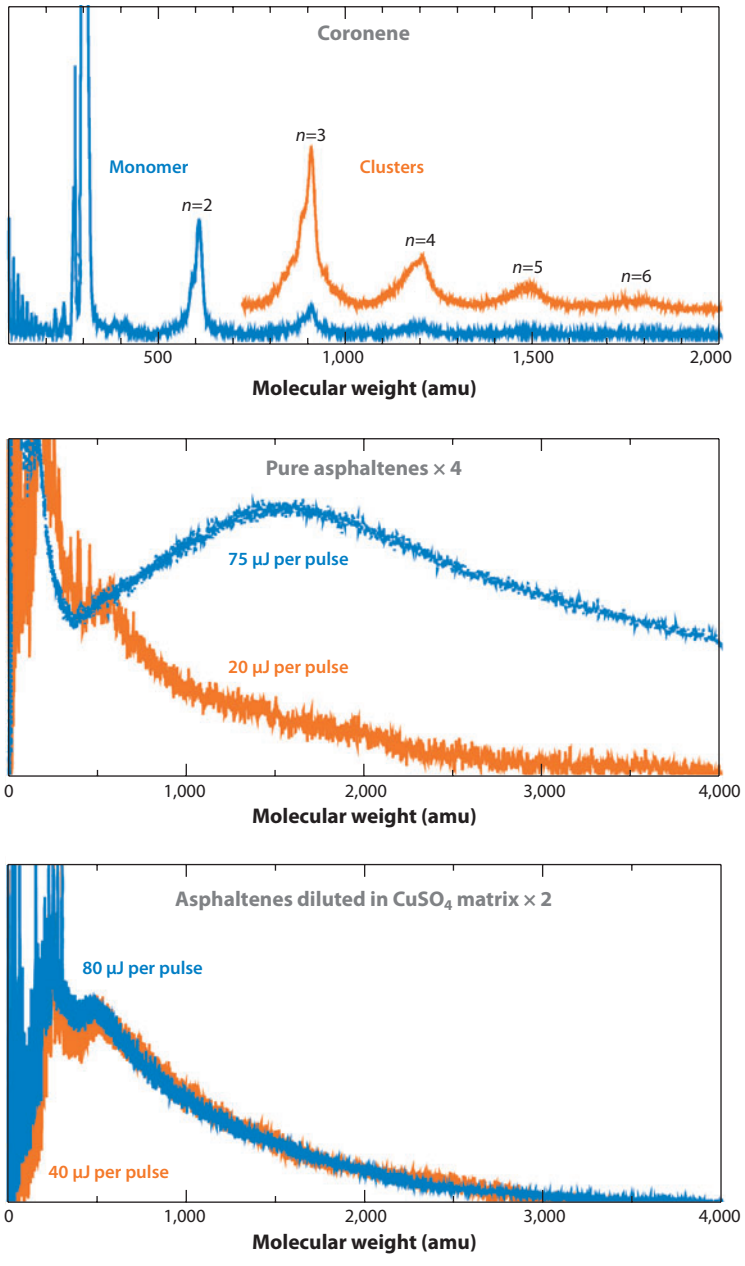

Figure 4

Laser desorption/ionization mass spectrometry measurements with high laser power can yield incorrect, excessive masses for known polycyclic aromatic hydrocarbons and asphaltenes (37–39). Low laser power and low surface coverage of asphaltenes are required to obtain the correct molecular weights of asphaltenes (37–39).

not cross-linked and, thus, there is one PAH per molecule. As in a quantum particle in a box, lower transition energies correspond to larger PAHs. This expected result has been established by molecular orbital calculations (51–54).

PAH ring geometry also influences optical spectra (51–55). X-ray Raman spectroscopy applied to asphaltenes has established that for asphaltene PAHs, the most stable aromatic sextet carbon dominates over isolated double-bond carbon (56, 57).

Direct molecular imaging of asphaltene molecules by scanning tunneling microscopy has established that asphaltene PAHs have roughly seven fused rings (58). High-resolution transmission electron microscopy has obtained similar results for petroleum asphaltenes, with somewhat smaller PAHs for coal-derived asphaltenes (59). Results obtained from Raman spectroscopy of asphaltenes are consistent with PAHs having seven fused rings (60, 61).

Calculated optical spectra of asphaltenes, based on molecular orbital calculations of 523 PAHs with a distribution peaked at seven fused rings, are close to observed spectra (**Figure 5**). Asphaltene optical absorption spectra obey the Urbach tail formalism, which is a result from solid-state physics that relates the well-ordered population distributions of absorbers to their corresponding spectra

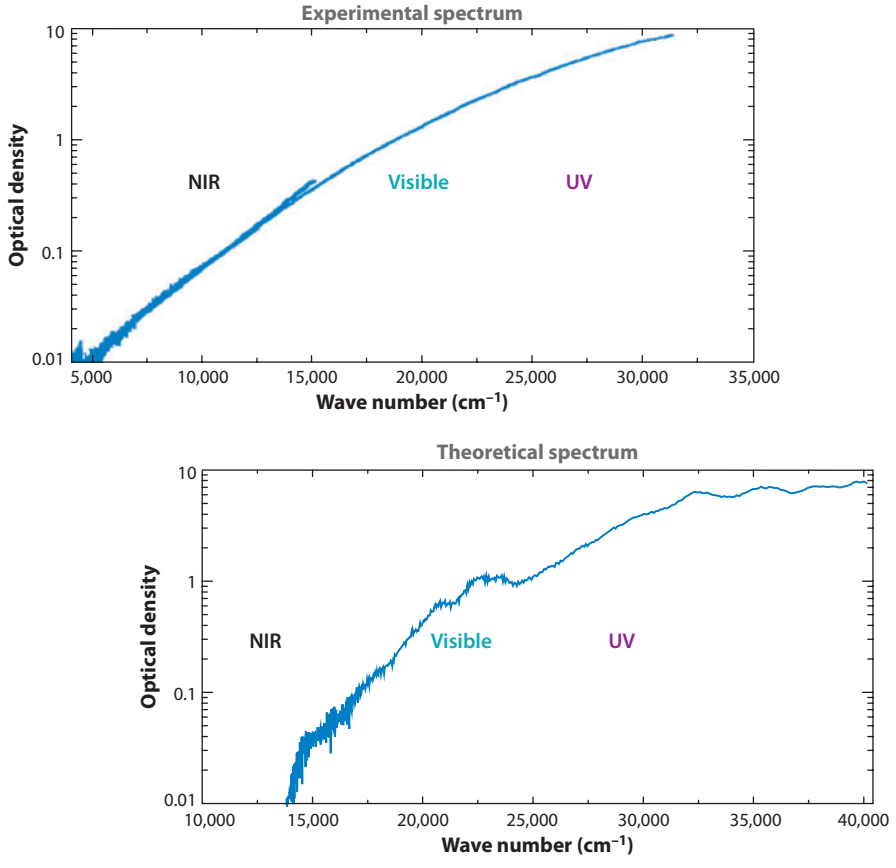

Figure 5

By use of an asphaltene polycyclic aromatic hydrocarbon distribution with 7 fused rings maximum, ranging roughly from 4 to 10 fused rings, molecular orbital calculated spectra match measured spectra across the near-infrared (NIR), visible, and ultraviolet (UV) wavelengths (51–53).

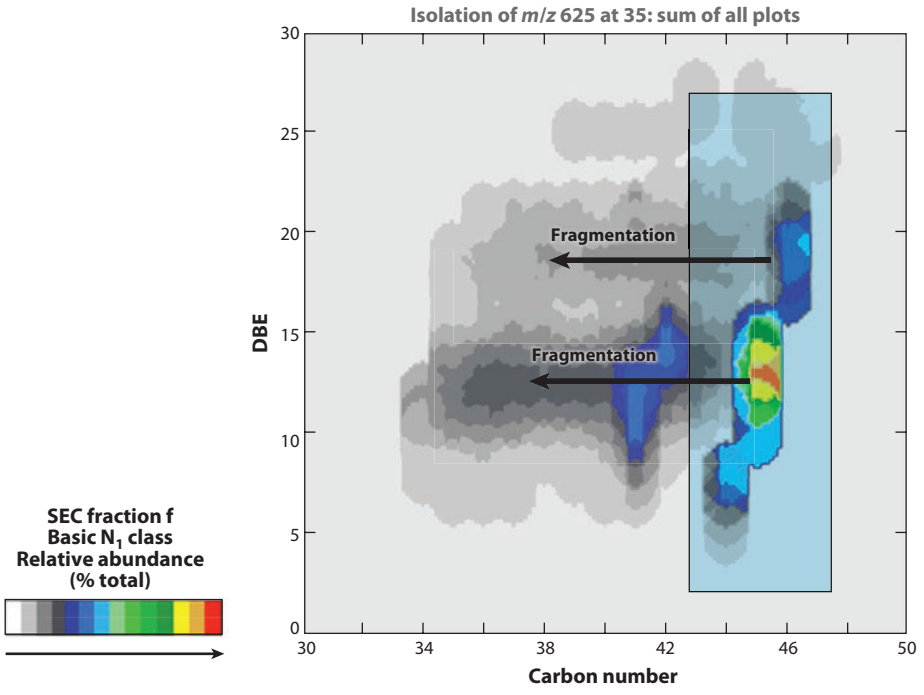

Figure 6

Gas-phase, unimolecular decomposition of asphaltene molecules via collision with helium gas. Fragmentation causes a loss of carbon but not a reduction in aromaticity, which is consistent only with the island molecular architecture (67, 68).

(62, 63). Asphaltene fluorescence spectra (64) and the absorption spectra (65, 66) show that small aromatics are missing in asphaltenes.

In agreement with TRFD studies, several recent experiments involving the unimolecular decomposition of asphaltenes reveal that the island model dominates. **Figure 6** shows results from an experiment that used FT-ICR MS to analyze unimolecular decomposition of asphaltenes by collision with helium gas (67, 68). Only alkane fragments are cleaved off, rather than alkane plus some aromatic carbon; this finding is consistent only with the island model (**Figure 3**) (67, 68).

In addition, L^2MS has been utilized on ~22 island and archipelago model compounds and on asphaltenes (41a). These studies show that asphaltenes and island model compounds do not undergo fragmentation (**Figure 7**) even under harsh fragmentation conditions, whereas archipelago model compounds fragment readily with increasing laser power. Recent LIAD EI MS fragmentation analysis yielded similar results (47). Independent of whether fragmentation is induced by helium collision, electron collision, or photoabsorption, island models and asphaltenes are stable, whereas archipelago models are unstable. Herein lies the likely explanation for the low archipelago abundance in asphaltenes: instability.

Petroleum asphaltenes consist of approximately 40% to 45% aromatic carbon; the remainder is aliphatic, as shown by ^{13}C NMR (69). Alkane chains are an average of four to five carbons long, as has been demonstrated by integrated IR and NMR studies (69). Naphthenic rings are fused to aromatic rings, as deduced from observations of active hydrogen in asphaltene (70). The aromatic ring system is also where almost all the nitrogen (~1% by mass) is located, as shown by X-ray absorption near-edge structure (XANES); both basic pyridinic nitrogen and acidic pyrrolic

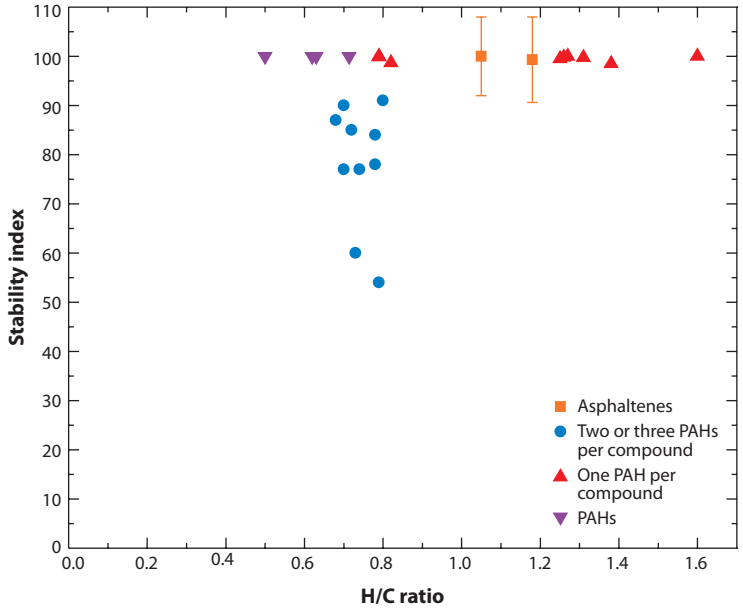

Figure 7

Two-step laser mass spectroscopy studies show that asphaltenes and island model compounds are very stable against fragmentation, independent of the hydrogen-to-carbon (H/C) ratio. Archipelago model compounds are much less stable (41a). The stability index is a measure of fragmentation tendency at low versus high laser power. Asphaltenes exist for geologic time and thus must be stable. Abbreviation: PAH, polycyclic aromatic hydrocarbon.

nitrogen are present (71). Sulfur XANES shows that most of the several percent sulfur consists of thiophene- and sulfide-type groups and generally a small fraction of sulfoxide (72, 73). Oxygen content is generally low in asphaltenes and can be found in various polar groups (42–45).

A significant fraction of dissolved organic matter (DOM) from deep ocean waters and from brine pools on the seafloor comes from natural oil seeps and waters associated with crude oil (74–76). Moreover, ESI combined with FT-ICR MS shows that such DOM consists of PAHs with carboxylate substituents (74–76); the PAHs are similar to those found in asphaltenes (76). Similar DOM chemical structures have been found in hydrothermal vents (P.E. Rossel, T. Dittmar, O.C. Mullins, L. Goual & N. Dubilier, manuscript submitted).

6. ASPHALTENE NANOAGGREGATES

The asphaltene PAH in the molecular interior is the primary site of intermolecular attraction (**Figure 3**) from both London dispersion forces and limited sites with dipoles. The asphaltene molecular exterior, with alkane substituents, yields steric repulsion. Consequently, there are two primary predictions, both of which have been observed: (*a*) The aggregation number of the nanoaggregate should be less than 10, and (*b*) there should be a single, somewhat disordered stack in a nanoaggregate. Asphaltenes can be obtained from the resid from thermal processing of coal-derived liquids; coals start with little alkane, and thermal processing leads to alkane removal. The much smaller molecular and PAH sizes of coal-derived asphaltenes arise from their smaller alkane fraction; the smaller repulsive forces balance the smaller attractive forces (5). The balance is

mandated by the asphaltene solubility classification. Petroleum-derived resid asphaltenes exhibit the same effects (26), which are consistent only with the island model (5). Thermal processing of the resid leads to removal of peripheral alkane groups; thus, smaller PAHs are mandated to maintain the asphaltene solubility classification.

Small-angle X-ray scattering (SAXS) and small-angle neutron scattering (SANS) have established that asphaltenes are nanosized colloids (77–86; J. Eyssautier, P. Levitz, D. Espinat, J. Jestin & J. Gummel, manuscript submitted). The smallest structures remain even at elevated temperatures (78, 79), indicating tight binding. High-quality (high-Q) ultrasonics studies were the first experiments to correctly measure the critical nanoaggregate concentration of asphaltenes (CNAC) (87, 88). The ultrasonic velocity, u, is given by $\sqrt{\frac{1}{\rho\beta}}$, where ρ is density and β is compressibility. Compressibility is a differential quantity and thus is very sensitive to onset, whereas density is an integral quantity and therefore is much less sensitive to the CNAC. The CNAC is obtained as a change in slope of sonic velocity versus asphaltene concentration (**Figure 8**) (87, 88). The CNAC is analogous to the critical micelle concentration of a monodisperse standard surfactant. The term critical is used herein even though the transition from a true molecular solution to a nanoaggregate is narrow in concentration only for large aggregation numbers (89), yet asphaltenes have small aggregation numbers. Fluorescence measurements indicate that the initial aggregation of asphaltenes is ~50 mg liter^{-1} (90), whereas the CNAC, at which aggregate growth shuts off, is ~100 mg liter^{-1} (87, 88). The nonlinearities of asphaltene fluorescence measurements associated with lifetime (27, 28), spectral energy transfer (91), and quenching (92) render fluorescence sensitive primarily to the initiation of aggregation.

Direct current (DC) conductivity measurements of CNAC match those from high-Q ultrasonics (**Figure 8**) (93). DC conductivity measurements are sensitive only to the 10^{-5} mass fraction of asphaltene molecules that is charged in toluene solution (93, 94). Ion mobility is reduced at CNAC and is related to the change in Stokes's drag, $6\pi\eta r/\mathrm{k}T$, where r is the molecular or aggregate size, η is viscosity, k is Boltzmann's constant, and T is temperature. The measured reduction in volume at the CNAC is a factor of six, which then becomes the estimate of the aggregation number (93). Alternating current conductivity measurements confirm the values of the CNAC and rely on changes in the dielectric response upon nanoaggregate formation (95).

NMR measurements clearly exhibit the CNAC, where the change in rotational relaxation at the CNAC yields a huge change in the hydrogen index (96). In addition, NMR diffusion measurements also exhibit the same CNAC (96). Centrifugation experiments show that the fraction of sedimented asphaltene changes dramatically at the CNAC (97, 97a). Moreover, these results are consistent with small (<10) aggregation numbers of asphaltene nanoaggregates (97a). Surface-tension measurements had been misinterpreted as giving a CNAC (or critical micelle concentration) at a 20-times-higher concentration (98). That concentration is the clustering concentration, discussed in the next section (99).

By contrasting the absolute cross sections obtained from SAXS and SANS, one can determine the structure and length scale of the nanoaggregates (**Figure 9**). X-ray scattering occurs preferentially from electrons, and therefore from the aromatic core of the nanoaggregate, whereas neutrons preferentially scatter from hydrogen, and therefore from the peripheral alkyl substituents (86). The deviation of SAXS from SANS data increases at distances smaller than ~14 Å, which is the size of the seven-fused-ring PAH (86).

In addition, a combined treatment of SANS and SAXS data (J. Eyssautier, P. Levitz, D. Espinat, J. Jestin & J. Gummel, manuscript submitted), as well as a detailed study of SANS data (84), finds that there is only a single (cylindrical) PAH stack in the asphaltene nanoaggregate (**Figure 9**). The stack is somewhat disordered, with solvent entrainment in the nanoaggregate, as shown by

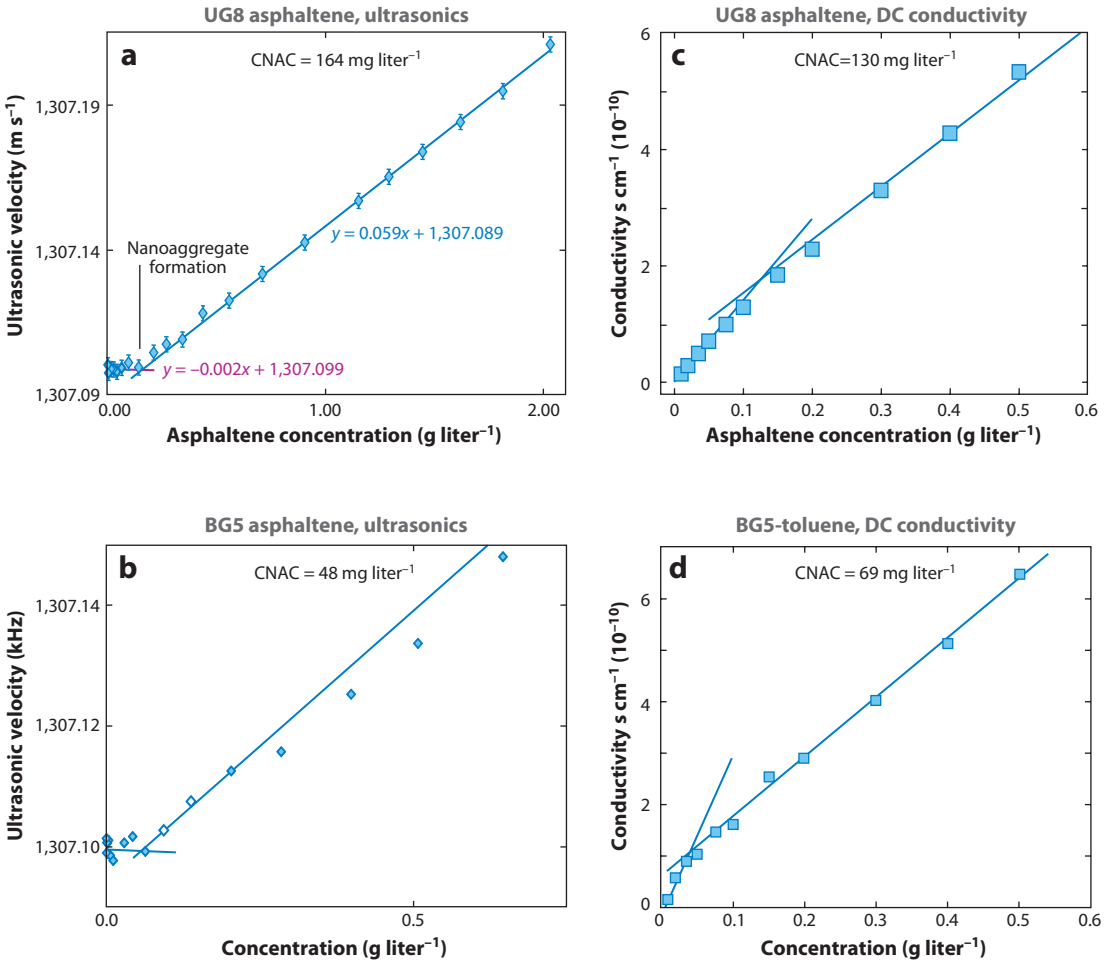

Figure 8

Critical nanoaggregate concentration (CNAC) of asphaltenes. (*a*,*b*) High-quality (high-*Q*) ultrasonics (87, 88). (*c*,*d*) Direct current (DC) conductivity (93). The break in the ultrasonic velocity and DC conductivity curves show the CNAC. The straight line of the ultrasonic velocity and DC conductivity curves above the CNAC indicates the nanoaggregate size is independent of the concentration above CNAC. For two different asphaltenes, the CNACs differ somewhat, as shown by consistent high-*Q* ultrasonics data and DC conductivity data. Hollow points were not used in either slope determination.

both SANS (85) and Langmuir-Blodgett film studies (65) of asphaltenes. Atomic force microscopy measurements of the thickness of Langmuir-Blodgett films of asphaltenes yield ~2 nm (65, 66). Surface-compression analyses of asphaltenes dissolved in both toluene and in chloroform show that the area per molecule is roughly one-tenth of the expected result, thus yielding an estimate of 10 for the aggregation number (65, 66).

7. CLUSTERS OF ASPHALTENE NANOAGGREGATES

At significantly higher concentrations than the CNAC, a secondary aggregation process takes place: the clustering of nanoaggregates. At the critical clustering concentration (CCC), a dramatic change in flocculation kinetics occurs (**Figure 10**) (100, 101).

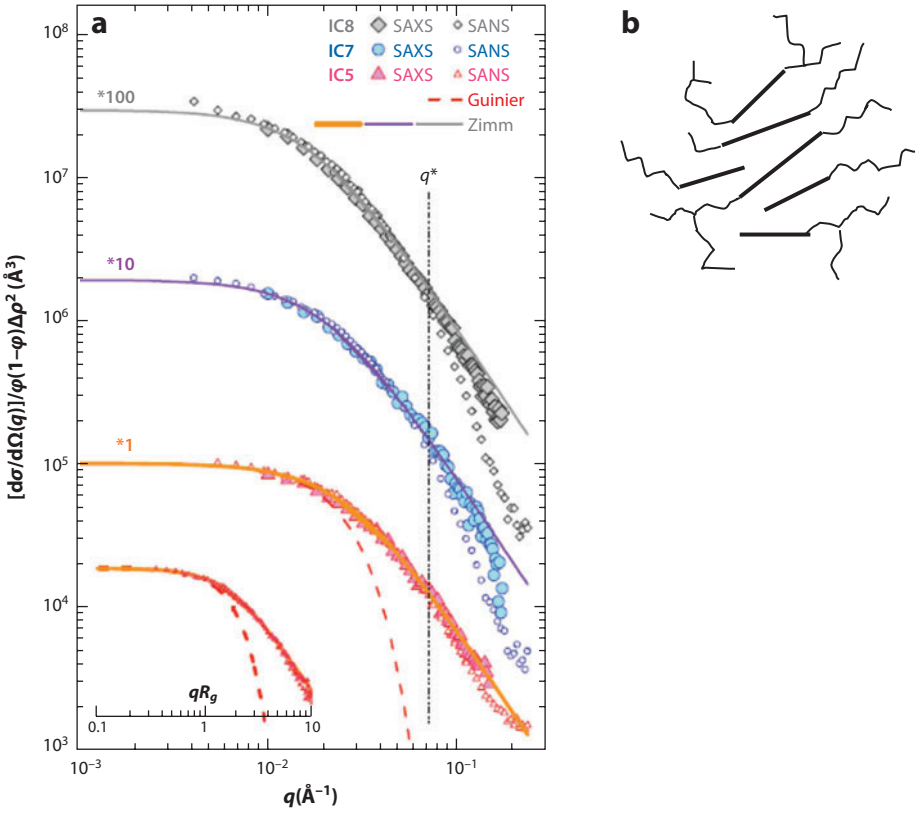

Figure 9

(*a*) Comparison between small-angle X-ray scattering (SAXS; *solid points*) and small-angle neutron scattering (SANS; *hollow points*) spectra. Variations of the normalized cross section $I(q)/\phi\Delta\rho^2$ as a function of the wave-scattering vector q for solutions of different asphaltenes in toluene. The dotted and solid lines represent the Guinier and Zimm approximations, respectively, in the small-q domain (86). The contrast between SAXS sensitivity to electron density, and thus the polycyclic aromatic hydrocarbon (PAH) stack, versus the SANS sensitivity to hydrogen, and thus the peripheral alkanes, gives the length scale of the interior PAH stack of the nanoaggregate: approximately 14 Å (86). (*b*) Proposed asphaltene nanoaggregate.

Below the CCC, *n*-heptane addition causes flocculation that is governed by diffusion-limited aggregation: The nanoaggregates stick upon collision. Above the CCC, the same flocculation process is governed by reaction-limited aggregation: The clusters are fractal (78, 102) and are loosely bound, requiring higher concentrations to form. Clusters need a morphological change at the interface to stick, yielding reaction-limited aggregation kinetics (W.W. Mullins, private communication). Other flocculation behaviors change dramatically at the CCC (103).

DC conductivity experiments show that such clusters have aggregation numbers less than 10 (97a). As with the CNAC, a break in the DC conductivity curve occurs at the CCC, in agreement with flocculation studies; the change in the slope enables size determination. An increase in entropy contributes to nanoaggregate formation (96) and perhaps to cluster formation (104). A limited cluster size, determined by DC conductivity studies (97a) and oil field studies (105), may result if entropy both helps form the clusters by excluded solvent (104) and limits cluster growth by favoring large numbers of clusters.

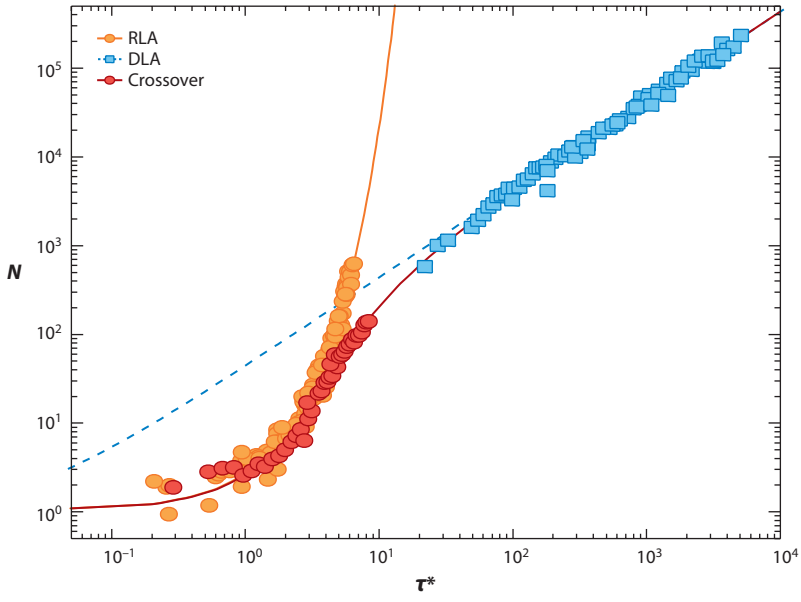

Figure 10

The aggregation number N as a function of the scaled time τ^*. Flocculation data for the addition of *n*-heptane to different asphaltene/toluene solutions. Orange circles represent data for a 10 g liter^{-1} asphaltene/toluene solution that exhibits reaction-limited aggregation (RLA). Solid squares represent data for a 1 g liter^{-1} asphaltene/toluene solution that exhibits diffusion-limited aggregation (DLA). Solid circles represent data for a 5 g liter^{-1} asphaltene/toluene solution that exhibits crossover aggregation kinetics (101).

Ultrafiltration studies with pores as small as 30 nm show that no asphaltene is retained—neither with natural crude oils nor with asphaltene/toluene solutions that greatly exceeded the clustering concentration. Thus, clusters are significantly smaller than 30 nm (106).

8. OIL FIELD STUDIES

The largest technical uncertainty in the oil industry remains the subsurface reservoir (9, 107). In an extreme description, a reservoir might resemble a kitchen sponge in which all the permeable zones are connected. Alternatively, a reservoir might resemble a spool of bubble wrap, in which all the wells intersect and drain only very small pockets of fluid. **Figure 11** shows the upper and lower horizons of a reservoir located at a total depth of more than 20,000 feet and under 4,000 feet of water. The field has been tilted by buoyant salt that creates faults. Fault transmissivity for fluid flow is generally the greatest risk factor in deepwater development. The reservoir crude oils have a low gas-to-oil ratio (GOR) and, consequently, are characterized by small-GOR gradients (109). Thus, in this case, GOR is not a useful property for the interrogation of reservoir connectivity.

Crude oil liquids and gases can be treated with variations of the van der Waals equation of state (109, 110). In contrast, until recently the molecular and colloidal structure of asphaltenes in crude oil were unknown; consequently, the gravity term was unknown, which precluded predictive modeling of asphaltenes in reservoirs. Nevertheless, understanding asphaltene gradients is vital, in part because differing asphaltene content creates orders-of-magnitude variations in viscosity (111). Using the modified Yen model, investigators have finally modeled heavy ends in crude oils (10).

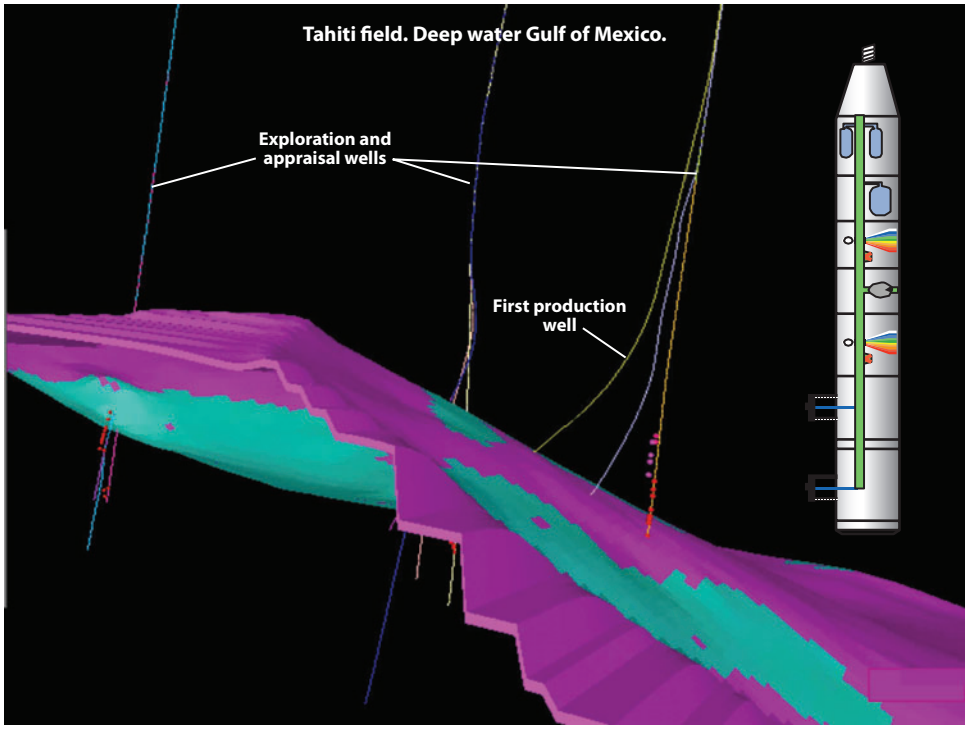

Figure 11

The horizons of a deepwater reservoir in the Tahiti oil field, Gulf of Mexico. The oil field is tilted due to sections that are uplifted by buoyant salt, which creates faults in the field. The greatest risk factor in this reservoir is whether the faults are sealing or transmissive for fluid flow. The asphaltenes are equilibrated across the reservoir, indicating connectivity (108), which was subsequently proved in production (105). A schematic of a tool for measuring fluid properties in oil wells is also shown.

All three structures that constitute the modified Yen model—namely asphaltene molecules, nanoaggregates, and clusters of nanoaggregates—have now been observed in various reservoir crude oils (105). A significant technological development, DFA, enabled such measurements (**Figure 11**) (9), the basis of which is primarily visible–near-IR spectroscopy. DFA methods have determined relative asphaltene content through the measurement of color at various wavelengths (63); color and asphaltene content have strict linearity (52, 108). Near-IR spectroscopy can also determine other fluid properties, such as GOR, by exploiting the different energies of the two-stretch overtone peaks for the CH_4, CH_3, and CH_2 groups (112, 113).

Light crude oils or condensates with an asphaltene fraction of $\ll$1% can contain true molecular solutions of the heavy ends of asphaltenes (**Figure 12*a***) (114). There are numerous instances in which nanoaggregates are the dominant form of asphaltenes in stable black oils, with asphaltene mass fractions of a few percent (**Figure 12*b***) (115–117). In heavy oils and in unstable black oils, in which asphaltene precipitation is problematic, asphaltene clusters can occur and dominate (**Figure 12*c***) (105). **Figure 12*d*** shows a series of crude oils for a single oil column, depicting dramatic, nonequilibrium reservoir fluid variations (9, 107). The use of new asphaltene modeling can establish whether asphaltenes are equilibrated across the reservoir; if they are equilibrated, massive fluid flow is required, so reservoir connectivity is implied. Objects measuring ~1 nm,

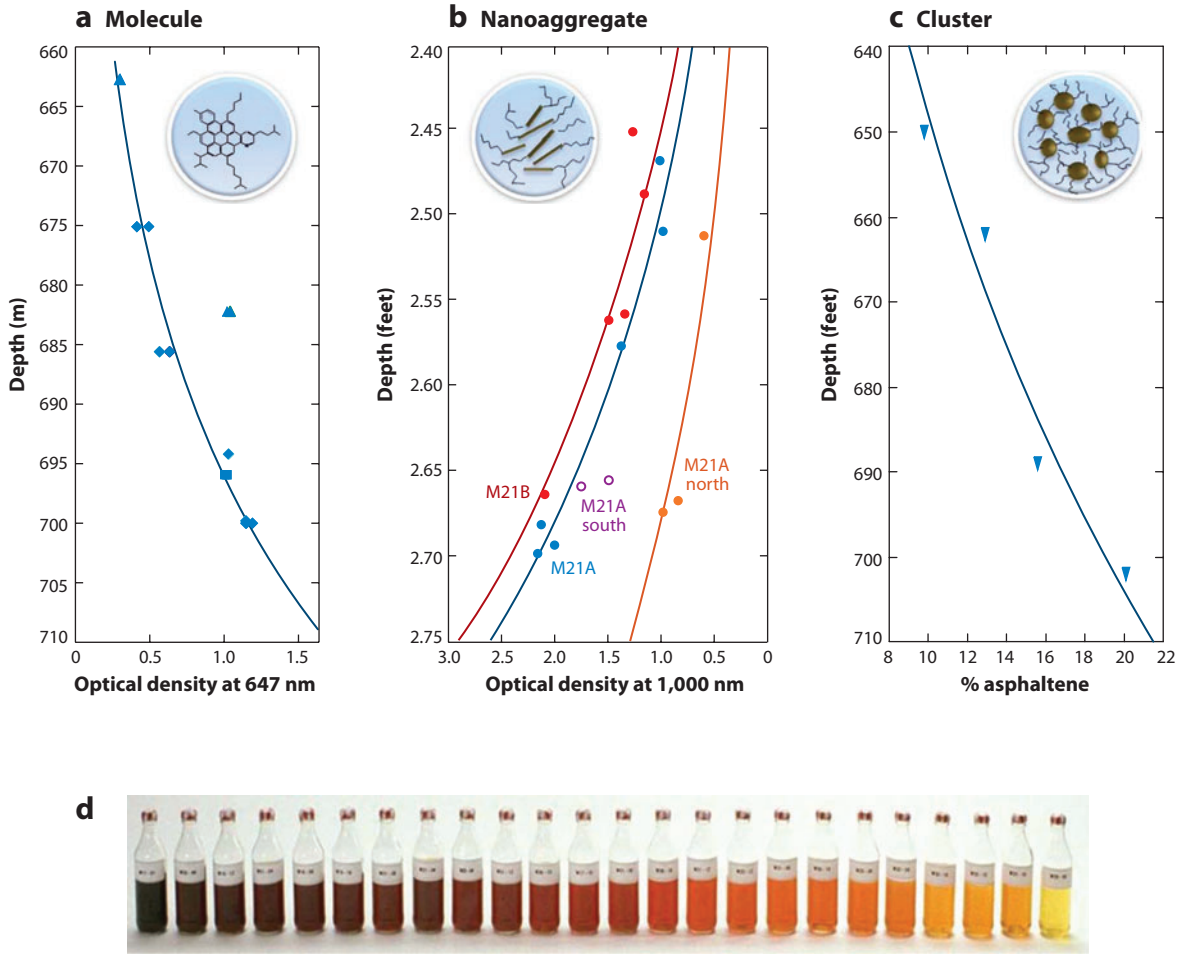

Figure 12

Asphaltene gradients in oil reservoirs. (*a*) For light oils (asphaltene content ≪1%), the asphaltenes are dispersed as a true molecular solution (114). (*b*) For stable black oils, asphaltenes are dispersed as nanoaggregates (114). (*c*) For heavy oils (asphaltene content ~10%) and unstable black oils, asphaltenes are dispersed as clusters of nanoaggregates (105). (*d*) A series of oil samples from a single oil reservoir, showing huge nonequilibrium asphaltene variations.

namely asphaltenes, are being used to determine connectivity in oil reservoirs with length scales of ~10 km, or 13 orders of magnitude larger than the asphaltenes (8, 105, 114).

Laboratory centrifugation of a live black oil with dissolved gases exhibits similar gradients (**Figure 13**) (118). The asphaltenes exhibit a large (10-fold) gradient due to both the gravity term and the solubility term from the GOR gradient (118). The resin gradient is much smaller, which indicates that bulk resins are not attached to the asphaltenes.

9. INTERFACIAL SCIENCE

The modified Yen model provides a framework in which to understand the interfacial science of asphaltenes. Sum frequency generation (SFG) reveals that asphaltenes in a Langmuir-Blodgett

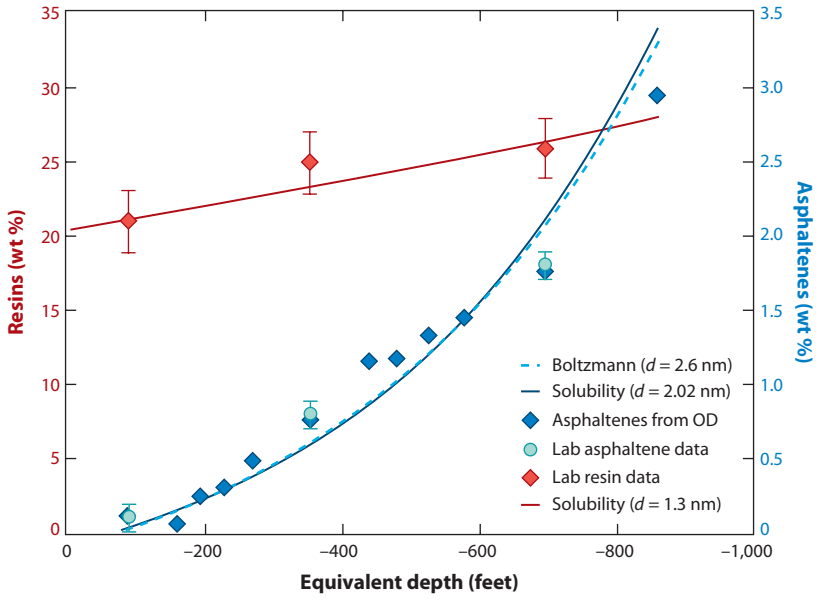

Figure 13

Asphaltene and resin gradients produced by centrifugation and fitted to a solubility model. Asphaltenes exhibit a huge gradient, whereas bulk resins exhibit a small gradient; this finding indicates that bulk resins are not associated with asphaltenes. The resin particle is ~1.3 nm, and the asphaltene nanoaggregate is ~2.0 nm. These results are in agreement with the modified Yen model (118). Abbreviation: OD, optical density.

film exhibit a high degree of molecular orientation, which is consistent with the island molecular architecture (**Figure 14**). The asphaltene PAH is in the plane of the film, and the alkanes are largely perpendicular to the surface (118a). Above CNAC, nanoaggregates go to the interface and their peripheral alkanes load on the surface, which explains the reduction in surface (99).

Below and above the CCC, there is a fundamental change in the Langmuir film morphology that reflects the different rheologies (**Figure 15**) of nanoaggregates versus clusters at the interface (119). Other studies of Langmuir films and Langmuir-Blodgett films of asphaltenes at concentrations below the CCC show (*a*) film thicknesses of ~2 nm and (*b*) aggregation numbers of less than 10, which are expected for nanoaggregates (65, 66). Many studies show that asphaltenes (120, 121) and other petroleum components (122) are crucial for water-in-oil emulsion stability. In particular, surface active components can be physically separated through the use of a heavy water technique (122, 123) that allows for detailed analysis (124). For crude oils, invert emulsions are stabilized because the surfactants are in the oil phase, which precludes water droplet coalescence but allows oil droplet coalescence.

10. THEORY: PHASE BEHAVIOR AND GRADIENTS

Asphaltene-phase behavior can be treated within the Flory-Huggins polymer framework (125, 126, 127). Asphaltene molecules are not of polymer size, but asphaltene nanoaggregates and clusters are large compared with solvent molecules. The corresponding Gibbs free energy of mixing (ΔG_{mixing}) for polymers is used, and the interaction parameter χ incorporates the Hildebrand

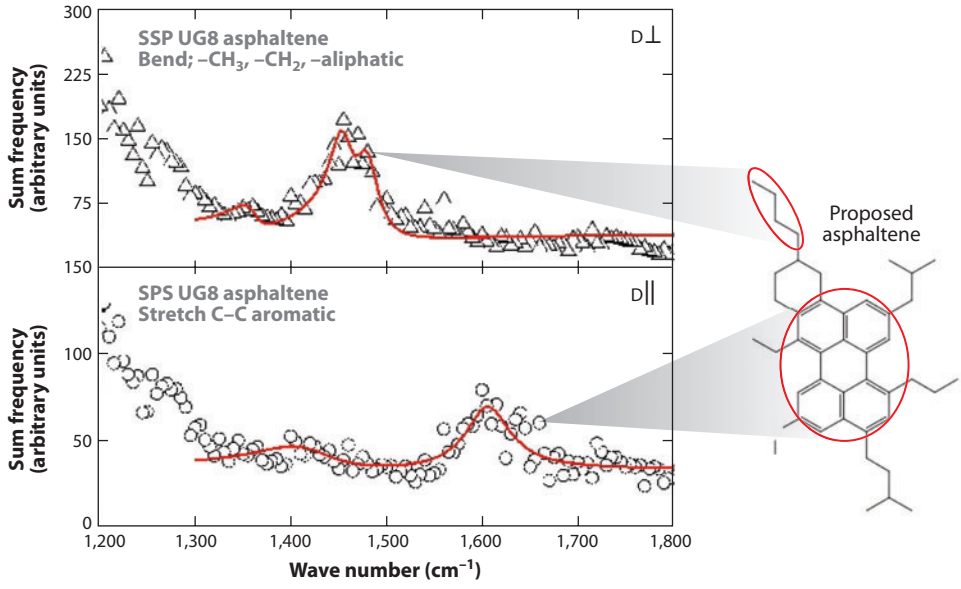

Figure 14

Sum frequency generation (SFG) data for a Langmuir film of UG8 asphaltene on water prepared from a ~0.2 g liter^{-1} toluene solution (118a). The SFG data show that the asphaltene polycyclic aromatic hydrocarbon is parallel to the interface and that the alkanes are perpendicular to it. Such strong alignment is consistent with the island molecular architecture hypothesis. S and P represent the two plane polarizations for the optical beams.

solubility parameter δ for asphaltenes and maltenes:

$$\Delta G_{mixing} = RT\,(n_m \ln \phi_m + n_a \ln \phi_a + n_m \phi_a \chi),$$

where n refers to moles; ϕ is the volume fraction; the subscripts m and a refer to maltene and asphaltene, respectively; and

$$\chi = \frac{v_m}{RT}(\delta_a - \delta_m)^2.$$

The parameter δ is given in terms of the energy of vaporization ΔU and the molar volume v: $\delta = \sqrt{\frac{\Delta U}{v}}$ (125). The Flory-Huggins approach successfully treats the onset of asphaltene flocculation for differing alkane solvents. Flocculation kinetics vary dramatically, depending on conditions (128). Other, related formalisms have been very successful in accounting for asphaltene-phase behavior (129, 130).

To model asphaltene gradients in oil reservoirs (**Figure 12**), the Flory-Huggins formalism can be coupled with a gravity term that incorporates the modified Yen model (10). For a homogeneous liquid phase, the gravity term dominates the asphaltene concentration C at height h (versus a reference value of zero), which is given by a Boltzmann distribution where Archimedes buoyancy gives the energy: $C_h/C_0 = \exp\{-V\Delta\rho g h/kT\}$, where V is the volume of the specific asphaltene species, $\Delta\rho$ is the density contrast between the asphaltene and the maltene, g is Earth's gravitational constant, k is Boltzmann's constant, and T is temperature (10).

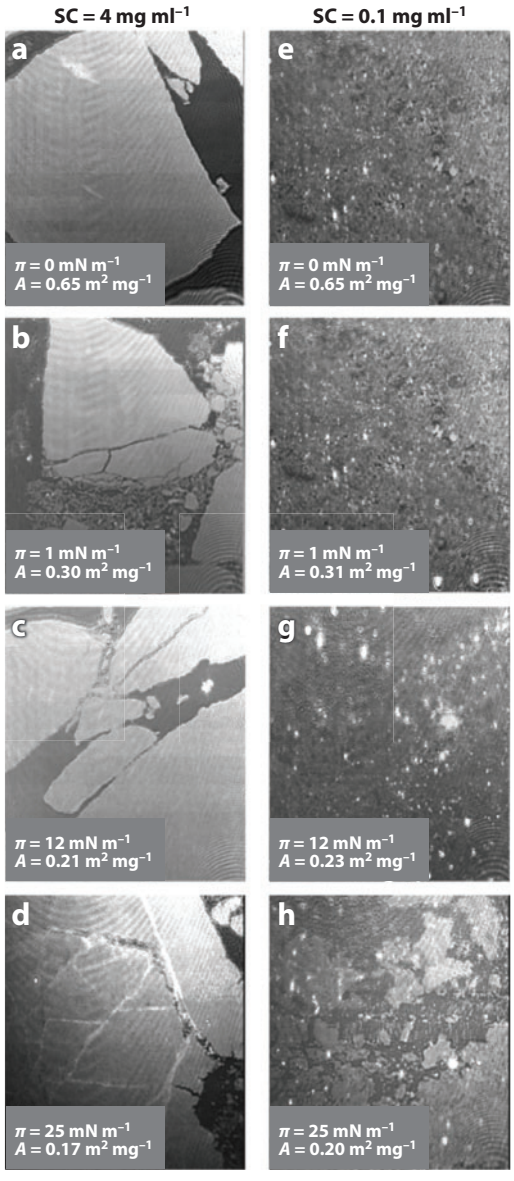

Figure 15

Brewster angle microscope images of asphaltene Langmuir films obtained from two different concentrations (SCs) at different surface pressures (π) on water (119). (*a*) 4 g liter^{-1}. (*b*) 0.1 g liter^{-1}. The corresponding values of specific area (in m^2 mg^{-1}) are also indicated. A huge morphology change is observed both above and below the critical clustering concentration (119). The images are 430 μm wide (119).

11. VISCOSITY

Asphaltenes have an enormous impact on viscosity. **Figure 16** shows that the viscosity of an asphaltenic system can vary by many orders of magnitude, depending on temperature (131) and asphaltene content (111, 131).

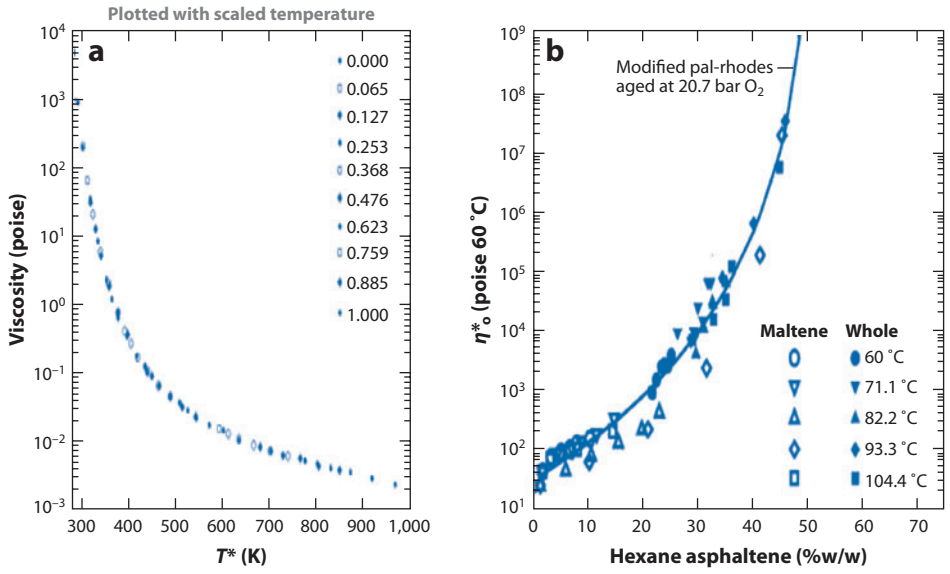

Figure 16

(*a*) C4 asphaltene solution in 1-methyl naphthalene; viscosity as a function of the temperature for varying dilutions and with the temperature multiplicatively scaled (131). (*b*) Viscosity versus C7 asphaltene concentration (111).

The viscosity variations of asphaltenic systems on temperature and concentration can be treated as a system of components with continuously varying glass-transition temperatures; more associative asphaltenes reflect a higher glass-transition temperature (131). Simple Arrhenius behavior (i.e., thermal activation), $\eta(T) = \eta_\infty \exp(E/kT)$, can describe the temperature dependency of the viscosity only over small temperature ranges (131). Over larger temperature ranges, a modified Arrhenius equation works well; varying asphaltene glass-transition temperatures are implicit (131):

$$\eta(T) = \eta_\infty \exp\{D/[(T/T_0)^{-1}]\}.$$

This simple formalism has been applied to high concentrations of asphaltic systems. The asphaltene chemical continuum is known from many studies and is a foundation of the variable glass-transition temperature approach.

12. RESINS AND ASPHALTENES

The role of resins in asphaltene science has long been unknown. Older micelle and surfactant models for resins are largely unsupported by evidence (125). Resins are not needed to stabilize asphaltene nanoaggregates in toluene, given that asphaltene nanoaggregates form in toluene without resins (5). Moreover, bulk resins do not associate with asphaltenes in live black oil centrifugation studies (**Figure 13**) (118). Centrifugation studies indicate that asphaltene nanoaggregates in live black oil contain ~15% *n*-heptane-soluble, *n*-pentane-insoluble material that could be termed either the heaviest resin or the lightest asphaltene (118). Ultrafiltration studies obtain similar conclusions regarding the extent of resin-asphaltene interaction, depending on conditions (132). The resins could be considered chain terminating, whereas the least soluble asphaltene fraction could be considered chain propagating (133). Petroporphyrins of varying associative strengths may play a similar role (I.D. Singh, D. Knepper, D. Savithri & P.K. Kilpatrick, manuscript

submitted). The definitions of asphaltene, toluene soluble, and *n*-heptane insoluble mostly—but not entirely—capture the largest aromatic component of crude oil that self-assemble.

13. CONCLUSIONS

Asphaltene science has undergone a renaissance in recent years. Many diverse studies have converged on a simple, hierarchical model of the molecular and colloidal structure of asphaltenes: the modified Yen model (also known as the Yen-Mullins model). Undoubtedly, complexities beyond the modified Yen model will emerge; nevertheless, it provides a framework for understanding large volumes of data. Asphaltene science is now reaching beyond traditional applications to encompass major new objectives in resource utilization. Reservoir characterization, a massive and vexing problem, is now being greatly enhanced by first-principles equations of state for asphaltenes, specifically employing the modified Yen model. Asphaltene interfacial science, a problematic frontier, can now be approached on a first-principles basis in part associated with bulk asphaltene properties, thereby simplifying analysis. Viscosity is treated with the compositional continuum of asphaltenes in simple ways. The molecular management of refining, a challenging objective, is being realized. These advances regarding the least tractable components of petroleum, the asphaltenes, have contributed greatly to the far-reaching vision of petroleomics: the establishment of predictive petroleum science based on structure-function relationships. After prolonged and unrelenting effort, chemical science has succeeded in characterizing the complex mixture represented by the asphaltenes. Nevertheless, many challenges await future generations of scientists devoted to understanding the asphaltenes.

DISCLOSURE STATEMENT

The author is not aware of any affiliations, memberships, funding, or financial holdings that might be perceived as affecting the objectivity of this review.

LITERATURE CITED

1. Mullins OC, Sheu EY, Hammami A, Marshall AG, eds. 2007. *Asphaltenes, Heavy Oils and Petroleomics*. New York: Springer
2. Mullins OC, Sheu EY, eds. 1998. *Structures and Dynamics of Asphaltenes*. New York: Plenum
3. Chilingarian GV, Yen TF, eds. 1978. *Bitumens, Asphalts and Tar Sands*. New York: Elsevier
4. Mullins OC, Martinez-Haya B, Marshall AG. 2008. Contrasting perspective on asphaltene molecular weight. *Energy Fuels* 22:1765–73
5. Mullins OC. 2010. The modified Yen model. *Energy Fuels* 24:2179–207
6. Marshall AG, Rodgers RP. 2008. Petroleomics: chemistry of the underworld. *Proc. Natl. Acad. Sci. USA* 105:18090–95
7. Ventura GT, Raghuraman B, Nelson RK, Mullins OC, Reddy CM. 2010. Compound class oil fingerprinting techniques using comprehensive two-dimensional gas chromatography (GC × GC). *Org. Geochem.* 41:1026–35
8. Peters KE, Walters CC, Moldowan JM. 2005. *The Biomarker Guide*. Cambridge, UK: Cambridge Univ. Press
9. Mullins OC. 2008. *The Physics of Reservoir Fluids: Discovery Through Downhole Fluid Analysis*. Houston: Schlumberger
10. Freed D, Mullins OC, Zuo J. 2010. Asphaltene gradients in the presence of GOR gradients. *Energy Fuels* 24:3942–49
11. Hammami A, Ratulowski J. 2007. Precipitation and deposition of asphaltenes in production systems: a flow assurance overview. See Ref. 1, pp. 617–60
12. Sjöblom J, Hemmingsen PV, Kallevik H. 2007. The role of asphaltenes in stabilizing water–in–crude oil emulsions. See Ref. 1, pp. 549–84

13. McLean JD, Spiecker PM, Sullivan AP, Kilpatrick PK. 1998. The role of asphaltenes in stabilizing water–in–crude oil emulsions. See Ref. 2, pp. 377–422
14. Kushnerick JD, Kennedy C. 2004. *Applications of compositional modeling in molecular management*. Presented at NPRA Plant Autom. Decis. Support Conf., 103rd, San Francisco
15. Shaw JM, Zou X. 2007. The phase behavior of heavy oil. See Ref. 1, pp. 485–506
16. Jones DM, Head IM, Gray ND, Adams JJ, Rowan AK, et al. 2008. Crude-oil biodegradation via methanogenesis in subsurface petroleum reservoirs. *Nature* 451:176–80
17. Valentine DL, Reddy CM, Farwell C, Hill TM, Pizarro O, et al. 2010. Asphalt volcanoes as a potential source of methane to late Pleistocene coastal waters. *Nat. Geosci.* 3:345–48
18. Dickie JP, Yen TF. 1967. Macrostrucutres of asphaltic fractions by various instrumental methods. *Anal. Chem.* 39:1847–52
19. Mullins OC. 2009. Rebuttal to Strausz et al. regarding time resolved fluorescence depolarization. *Energy Fuels* 23:2845–54
20. Strausz OP, Mojelsky TW, Lown EM. 1992. The molecular structure of asphaltene: an unfolding story. *Fuel* 71:1355–63
21. Groenzin H, Mullins OC. 1999. Asphaltene molecular size and structure. *J. Phys. Chem. A* 103:11237–45
22. Groenzin H, Mullins OC. 2000. Molecular sizes of asphaltenes from different origin. *Energy Fuels* 14:677–84
23. Buenrostro-Gonzalez E, Groenzin H, Lira-Galeana C, Mullins OC. 2001. The overriding chemical principles that define asphaltenes. *Energy Fuels* 15:972–78
24. Groenzin H, Mullins OC, Eser S, Mathews J, Yang MG, Jones D. 2003. Molecular size of asphaltene solubility fractions. *Energy Fuels* 17:498–503
25. Badre S, Goncalves CC, Norinaga K, Gustavson G, Mullins OC. 2006. Molecular size and weight of asphaltene and asphaltene solubility fractions from coals, crude oils and bitumen. *Fuel* 85:1–11
26. Buch L, Groenzin H, Buenrostro-Gonzalez E, Andersen SI, Lira-Galeana C, Mullins OC. 2003. Effect of hydrotreatment on asphaltene fractions. *Fuel* 82:1075–84
27. Wang X, Mullins OC. 1994. Fluorescence lifetime studies of crude oils. *Appl. Spectrosc.* 48:977–84
28. Owens P, Ryder AG, Blamey NJF. 2008. Frequency domain fluorescence lifetime study of crude petroleum oils. *J. Fluoresc.* 18:997–1006
29. Andrews AB, Guerra R, Mullins OC, Sen PN. 2006. Diffusivity of asphaltene molecules by fluorescence correlation spectroscopy. *J. Phys. Chem. A* 110:8095–97
30. Guerra R, Andrews AB, Mullins OC, Sen PN. 2007. Diffusivity of coal and petroleum asphaltene monomers by fluorescence correlation spectroscopy. *Fuel* 86:2016–20
31. Schneider M, Andrews AB, Mitra-Kirtley S, Mullins OC. 2007. Asphaltene molecular size from translational diffusion constant by fluorescence correlation spectroscopy. *Energy Fuels* 21:2875–82
32. Freed DE, Lisitza NV, Sen PN, Song YQ. 2007. Asphaltene molecular composition and dynamics from NMR diffusion measurements. See Ref. 1, pp. 279–96
33. Wargadalam VJ, Norinaga K, Iino M. 2002. Size and shape of a coal asphaltene studied by viscosity and diffusion coefficient measurements. *Fuel* 81:1403–7
34. Boduszynski MM. 1981. Asphaltenes in petroleum asphalts: composition and formation. In *Chemistry of Asphaltenes*, ed. JW Bunger, NC Li, pp. 119–35. Washington, DC: Am. Chem. Soc.
35. Miller JT, Fisher RB, Thiyagaranjan P, Winans RE, Hunt JE. 1998. Subfractionation and characterization of Mayan asphaltene. *Energy Fuels* 12:1290–98
36. Herod AA, Bartle KD, Kandiyoti R. 2008. Comment. *Energy Fuels* 22:4312–17
37. Hortal AR, Martínez-Haya B, Lobato MD, Pedrosa JM, Lago S. 2006. On the determination of molecular weight distributions of asphaltenes and their aggregates in laser desorption ionization experiments. *J. Mass Spectrom.* 41:960–68
38. Martínez-Haya B, Hortal AR, Hurtado PM, Lobato MD, Pedrosa JM. 2007. Laser desorption/ionization determination of molecular weight distributions of polyaromatic carbonaceous compounds and their aggregates. *J. Mass Spectrom.* 42:701–13
39. Hortal AR, Hurtado PM, Martínez-Haya B, Mullins OC. 2007. Molecular weight distributions of coal and petroleum asphaltenes from laser desorption ionization experiments. *Energy Fuels* 21:2863–68

40. Pomerantz AE, Hammond MR, Morrow AL, Mullins OC, Zare RN. 2008. Two-step laser mass spectrometry of asphaltenes. *J. Am. Chem. Soc.* 130:7216–17
41. Pomerantz AE, Hammond MR, Morrow AL, Mullins OC, Zare RN. 2009. Asphaltene molecular weight distribution determined by two-step laser mass spectrometry. *Energy Fuels* 23:1162–68
41a. Sabbah H, Morrow AL, Pomerantz AE, Zare RN. 2011. Evidence for island structures as the dominant architecture of asphaltenes. *Energy Fuels.* In press
42. Klein GC, Kim S, Rodgers RP, Marshall AG, Yen A, Asomaning S. 2006. Mass spectral analysis of asphaltenes. I. Compositional differences between pressure-drop and solvent-drop asphaltenes determined by electrospray ionization Fourier transform ion cyclotron resonance mass spectrometry. *Energy Fuels* 20:1965–72
43. Klein GC, Kim S, Rodgers RP, Marshall AG, Yen A. 2006. Mass spectral analysis of asphaltenes. II. Detailed compositional comparison of asphaltenes deposit to its crude oil counterpart for two geographically different crude oils by ESI FT-ICR MS. *Energy Fuels* 20:1973–79
44. Hughey CA, Rodgers RP, Marshall AG, Qian K, Robbins WR. 2002. Identification of acidic NSO compounds in crude oils of different geochemical origins by negative ion electrospray Fourier transform ion cyclotron resonance mass spectrometry. *Org. Geochem.* 33:743–59
45. Rodgers RP, Marshall AG. 2007. Petroleomics: advanced characterization of petroleum derived materials by Fourier transform ion cyclotron resonance mass spectrometry (FT-ICR MS). See Ref. 1, pp. 63–89
46. Pinkston DS, Duan P, Gallardo VA, Habicht SC, Tan X, et al. 2009. Analysis of asphaltenes and asphaltene model compounds by laser-induced acoustic desorption/Fourier transform ion cyclotron resonance mass spectrometry. *Energy Fuels* 23:5564–70
47. Borton D II, Pinkston DS, Hurt MR, Tan X, Azyat K, et al. 2010. Molecular structures of asphaltenes based on their ions' dissociation reactions in mass spectrometry. *Energy Fuels* 24:5548–59
48. Merdrignac I, Desmazieres B, Terrier P, Delobel A, Laprevote O. 2004. *Analysis of raw and hydrotreated asphaltenes using off-line and on-line SEC/MS coupling.* Presented at Int. Conf. Heavy Org. Depos., Los Cabos, Baja Calif., Mex., Nov. 14–19
49. Cunico RI, Sheu EY, Mullins OC. 2004. Molecular weight measurement of UG8 asphaltene by APCI mass spectroscopy. *Pet. Sci. Technol.* 22:787–98
50. Qian K, Edwards KE, Siskin M, Olmstead WN, Mennito AS, et al. 2007. Desorption and ionization of heavy petroleum molecules and measurement of molecular weight distributions. *Energy Fuels* 21:1042–47
51. Ruiz-Morales Y, Mullins OC. 2007. Polycyclic aromatic hydrocarbons of asphaltenes analyzed by molecular orbital calculations with optical spectroscopy. *Energy Fuels* 21:256–65
52. Ruiz-Morales Y, Wu X, Mullins OC. 2007. Electronic absorption edge of crude oils and asphaltenes analyzed by molecular orbital calculations with optical spectroscopy. *Energy Fuels* 21:944–52
53. Ruiz-Morales Y, Mullins OC. 2009. Simulated and measured optical absorption spectra of asphaltenes. *Energy Fuels* 23:1169–77
54. Ruiz-Morales Y. 2002. HOMO-LUMO gap as an index of molecular size and structure for polycyclic aromatic hydrocarbons (PAHs) and asphaltenes: a theoretical study. *J. Phys. Chem. A* 106:11283–308
55. Ruiz-Morales Y. 2004. The agreement between Clar structures and nucleus-independent chemical shift values in pericondensed benzenoid polycyclic aromatic hydrocarbons: an application of the Y-rule. *J. Phys. Chem. A* 108:10873–96
56. Bergmann U, Mullins OC, Cramer SP. 2000. X-ray Raman spectroscopy of carbon in asphaltene: light element characterization with bulk sensitivity. *Anal. Chem.* 72:2609–12
57. Bergmann U, Groenzin H, Mullins OC, Glatzel P, Fetzer J, Cramer SP. 2003. Carbon K-edge X-ray Raman spectroscopy supports simple yet powerful description of aromatic hydrocarbons and asphaltenes. *Chem. Phys. Lett.* 369:184–91
58. Zajac GW, Sethi NK, Joseph JT. 1994. Molecular imaging of petroleum asphaltenes by scanning tunneling microscopy: verification of structure from ^{13}C and proton NMR data. *Scan. Microsc.* 8:463–70
59. Sharma A, Groenzin H, Tomita A, Mullins OC. 2002. Probing order in asphaltenes and aromatic ring systems by HRTEM. *Energy Fuels* 16:490–96

60. Bouhadda Y, Bormann D, Sheu EY, Bendedouch D, Krallafa A, Daaou M. 2007. Characterization of Algerian Hassi-Messaoud asphaltene structure using Raman spectrometry and X-ray diffraction. *Fuel* 86:1855–64
61. Bouhadda Y, Fergoug T, Sheu EY, Bendedouch D, Krallafa A, et al. 2008. Second order Raman spectra of Algerian Hassi-Messaoud asphaltene. *Fuel* 87:3481–82
62. Mullins OC, Zhu Y. 1992. First observation of the Urbach tail in a multicomponent organic system. *Appl. Spectrosc.* 46:354–56
63. Mullins OC, Mitra-Kirtley S, Zhu Y. 1992. Electronic absorption edge of petroleum. *Appl. Spectrosc.* 46:1405–11
64. Ralston CY, Mitra-Kirtley S, Mullins OC. 1996. Small population of one to three fused-ring moieties in asphaltenes. *Energy Fuels* 10:623–30
65. Orbulescu J, Mullins OC, Leblanc RM. 2010. Surface chemistry and spectroscopy of UG8 asphaltene Langmuir film. Part 2. *Langmuir* 26:15265–71
66. Orbulescu J, Mullins OC, Leblanc RM. 2010. Surface chemistry and spectroscopy of UG8 asphaltene Langmuir film. Part 1. *Langmuir* 26:15257–64
67. McKenna AM, Purcell JM, Rodgers RP, Marshall AG. 2008. *Atmospheric pressure photoionization Fourier transform ion cyclotron resonance mass spectrometry for detailed compositional analysis of petroleum*. Presented at Int. Conf. Pet. Phase Behav. Fouling, 9th, Victoria, Can.
68. McKenna AM, Purcell JM, Rodgers RP, Marshall AG. 2009. *Atmospheric pressure photoionization Fourier transform ion cyclotron resonance mass spectrometry for detailed compositional analysis of petroleum*. Presented at Int. Conf. Pet. Phase Behav. Fouling, 10th, Rio de Janeiro, Brazil
69. Scotti R, Montanari L. 2008. Molecular structure and intermolecular interaction of asphaltenes by FT-IR, NMR and EPR. In *Structures and Dynamics of Asphaltenes*, ed. OC Mullins, EY Sheu, pp. 79–114. New York: Plenum
70. Gould KA, Wiehe IA. 2007. Natural hydrogen donors in petroleum resids. *Energy Fuels* 21:1199–204
71. Mitra-Kirtley S, Mullins OC, Chen J, van Elp J, George SJ, Cramer SP. 1993. Determination of the nitrogen chemical structures in petroleum asphaltenes using XANES spectroscopy. *J. Am. Chem. Soc.* 115:252–58
72. George GN, Gorbaty ML. 1989. Sulfur K-edge X-ray absorption spectroscopy of petroleum asphaltenes. *J. Am. Chem. Soc.* 111:3182–86
73. Waldo GS, Mullins OC, Penner-Hahn JE, Cramer SP. 1992. Determination of the chemical environment of sulphur in petroleum asphaltenes by X-ray absorption spectroscopy. *Fuel* 71:53–57
74. Dittmar T. 2008. The molecular level determination of black carbon in marine dissolved organic matter. *Org. Geochem.* 39:396–407
75. Koch BP, Dittmar T. 2006. From mass to structure: an aromaticity index for high-resolution mass data of natural organic matter. *Rapid Commun. Mass Spectrom.* 20:926–32
76. Dittmar T, Koch BP. 2006. Thermogenic organic matter dissolved in the abyssal ocean. *Mar. Chem.* 102:208–17
77. Yen TF, Erdman JG, Pollack SS. 1961. Investigation of the structure of petroleum asphaltenes by X-Ray diffraction. *Anal. Chem.* 33:1587–94
78. Sheu EY. 1995. Colloidal properties of asphaltenes in organic solvents. In *Asphaltenes: Fundamentals and Applications*, ed. EY Sheu, OC Mullins, pp. 1–52. New York: Plenum
79. Sheu EY. 2007. Petroleomics and characterization of asphaltene aggregates using small angle scattering. See Ref. 1, pp. 353–73
80. Wiehe IA, Liang KS. 1996. Asphaltenes, resins, and other petroleum macromolecules. *Fluid Phase Equilib.* 117:201–10
81. Barre L, Simon S, Palermo T. 2008. Solution properties of asphaltenes. *Langmuir* 24:3709–17
82. Fenistein D, Barre L. 2001. Experimental measurement of the mass distribution of petroleum asphaltene aggregates using ultracentrifugation and small-angle X-ray scattering. *Fuel* 80:283–87
83. Fenistein D, Barre L, Espinat D, Livet A, Roux J-N, Scarcella M. 1998. Viscosimetric and neutron scattering study of asphaltene aggregates in mixed toluene/heptane solvents. *Langmuir* 14:1013–20
84. Gawrys KL, Kilpatrick PK. 2005. Asphaltenic aggregates are polydisperse oblate cylinders. *J. Colloid Interface Sci.* 288:325–34

85. Gawrys KL, Blankenship GA, Kilpatrick PK. 2006. Solvent entrainment in and flocculation of asphaltenic aggregates probed by small-angle neutron scattering. *Langmuir* 22:4487–97
86. Barré L, Jestin J, Morisset A, Palermo T, Simon S. 2009. Relation between nanoscale structure of asphaltene aggregates and their macroscopic solution properties. *Oil Gas Sci. Technol.* 64:617–28
87. Andreatta G, Bostrom N, Mullins OC. 2005. High-*Q* ultrasonic determination of the critical nanoaggregate concentration of asphaltenes and the critical micelle concentration of standard surfactants. *Langmuir* 21:2728–36
88. Andreatta G, Goncalves CC, Buffin G, Bostrom N, Quintella CM, et al. 2005. Nanoaggregates and structure-function relations in asphaltenes. *Energy Fuels* 19:1282–89
89. Friberg SE. 2007. Micellization. See Ref. 1, pp. 189–202
90. Goncalves S, Castillo J, Fernandez A, Hung J. 2004. Absorbance and fluorescence spectroscopy on the aggregation of asphaltene-toluene solutions. *Fuel* 83:1823–28
91. Downare TD, Mullins OC. 1995. Visible and near-infrared fluorescence of crude oils. *Appl. Spectrosc.* 49:754–64
92. Ralston CY, Wu X, Mullins OC. 1996. Quantum yields of crude oils. *Appl. Spectrosc.* 50:1563–68
93. Zeng H, Song YQ, Johnson DL, Mullins OC. 2009. Critical nanoaggregate concentration of asphaltenes by low frequency conductivity. *Energy Fuels* 23:1201–8
94. Goual L. 2009. Impedance spectroscopy of petroleum fluids at low frequency. *Energy Fuels* 23:2090–94
95. Sheu EY, Long Y, Hamza H. 2007. Asphaltene self-association and precipitation in solvents, AC conductivity measurements. See Ref. 1, pp. 259–76
96. Freed DE, Lisitza NV, Sen PN, Song YQ. 2009. A study of asphaltene nanoaggregation by NMR. *Energy Fuels* 23:1189–93
97. Mostowfi F, Indo K, Mullins OC, McFarlane R. 2009. Asphaltene nanoaggregates and the critical nanoaggregate concentration from centrifugation. *Energy Fuels* 23:1194–200
97a. Goual L, Sedghi M, Zeng H, Mostowfi F, McFarlane R, Mullins OC. 2011. On the formation and properties of asphaltene nanoaggregates and clusters by DC-conductivity and centrifugation. *Fuel*. In press
98. Friberg SE, Mullins OC, Sheu EY. 2005. Surface activity of an amphiphilic association structure. *J. Dispers. Sci. Technol.* 26:513–15
99. Friberg SE, Al Bawab A, Abdoh AA. 2007. Surface active inverse micelles. *Colloid Polym. Sci.* 285:1625–30
100. Anisimov MA, Yudin IK, Nikitin V, Nikolaenko G, Chernoutsan A, et al. 1995. Asphaltene aggregation in hydrocarbon solutions studied by photon correlation spectroscopy. *J. Phys. Chem.* 99:9576–80
101. Yudin IK, Anisimov MA. 2007. Dynamic light scattering monitoring of asphaltene aggregation in crude oils and hydrocarbon solutions. See Ref. 1, pp. 439–66
102. Sheu EY. 2002. Petroleum asphaltene—properties, characterization, and issues. *Energy Fuels* 16:74–82
103. Oh K, Deo MD. 2007. Near infrared spectroscopy to study asphaltene aggregation in solvents. See Ref. 1, pp. 469–87
104. Jain S, Ginzburg VV, Jog P, Weinhold J, Srivastava R, Chapman WG. 2009. Modeling polymer-induced interactions between two grafted surfaces: comparison between interfacial statistical associating fluid theory and self-consistent field theory. *J. Chem. Phys.* 131:044908
105. Mullins OC, Freed DE, Zuo JY, Elshahawi H, Cribbs ME, et al. 2010. *Downhole fluid analysis coupled with asphalene nanoscience for reservoir evaluation*. Presented at SPWLA Annu. Technol. Conf., Perth, Aust.
106. Ching MJTM, Pomerantz AE, Andrews AB, Dryden P, Mullins OC, Harrison C. 2010. On the nanofiltration of asphaltene solutions, crude oils and emulsions. *Energy Fuels* 24:5028–37
107. Elshahawi H, Mullins OC, Hows M, Colacelli S, Flannery M, et al. 2009. *Reservoir fluid analysis as a proxy for connectivity in deepwater reservoirs*. Presented at SPWLA Annu. Technol. Conf., The Woodlands, TX
108. Mullins OC, Betancourt SS, Cribbs ME, Creek JL, Andrews BA, et al. 2007. The colloidal structure of crude oil and the structure of reservoirs. *Energy Fuels* 21:2785–94
109. Hoier L, Whitson C. 2001. Compositional grading, theory and practice. *Soc. Pet. Eng. Reserv. Eval. Eng.* 4:525–35

110. Ratulowski J, Fuex AN, Westrich JE, Sieler JJ. 2003. Theoretical and experimental investigation of isothermal compositional grading. Pap. SPE 84777. *Soc. Pet. Eng. Reserv. Eval. Eng.* 6:168–75
111. Lin MS, Lumsford KM, Glover CJ, Davison RR, Bullin JA. 1995. The effects of asphaltenes on the chemical and physical characteristics of asphalt. In *Asphaltenes: Fundamentals and Applications*, ed. EY Sheu, OC Mullins, pp. 155–76. New York: Plenum
112. Mullins OC, Daigle T, Crowell C, Groenzin H, Joshi NB. 2001. Gas-oil ratio of live crude oils determined by near-infrared spectroscopy. *Appl. Spectrosc.* 55:197–201
113. Mullins OC, Joshi NB, Groenzin H, Daigle T, Crowell C, et al. 2000. Linearity of alkane near-infrared spectra. *Appl. Spectrosc.* 54:624–29
114. Gisolf A, Dubost FX, Zuo JY, Williams S, Kristoffersen J, et al. 2009. *Real time integration of reservoir modeling and formation testing*. Pap. 121275. Presented at Soc. Pet. Eng. Eur./EAGE Annu. Conf. Exhib., Amsterdam
115. Betancourt SS, Dubost FX, Mullins OC, Cribbs ME, Creek JL, Mathews SG. 2007. *Predicting downhole fluid analysis logs to investigate reservoir connectivity*. Pap. 11488-MS. Presented at Soc. Pet. Eng. IPTC Conf. Dubai, UAE, Dec. 4–6
116. Betancourt SS, Ventura GT, Pomerantz AE, Viloria O, Dubost FX, et al. 2009. Nanoaggregates of asphaltenes in a reservoir crude oil. *Energy Fuels* 23:1178–88
117. Pomerantz AE, Ventura GT, McKenna AM, Cañas JA, Auman J, et al. 2010. Combining biomarker and bulk compositional gradient analysis to assess reservoir connectivity. *Org. Geochem.* 41:812–21
118. Indo K, Ratulowski J, Dindoruk B, Gao J, Zuo JY, Mullins OC. 2009. Asphaltene nanoaggregates measured in a live crude oil by centrifugation. *Energy Fuels* 23:4460–69
118a. Andrews AB, McClelland A, Korkeila O, Demidov A, Krummel A, et al. 2011. Molecular orientation of asphaltenes and PAH model compounds in Langmuir-Blodgett films using sum frequency generation spectroscopy. *Langmuir*. In press
119. Lobato MD, Pedrosa JM, Möbius D, Lago S. 2009. Optical characterization of asphaltenes at the air-water interface. *Langmuir* 25:1377–84
120. Spiecker PM, Gawrys KL, Trail CB, Kilpatrick PK. 2003. Effects of petroleum resins on asphaltene aggregation and water-in-oil emulsion formation. *Colloids Surf. A* 220:9–27
121. Sjöblom J, Sæther Ø, Midttun Ø, Ese M-H, Urdahl O, Førdedal H. 1998. Asphaltene and resin stabilized crude oil emulsions: experimental characterization and destabilizaiton. See Ref. 2, pp. 337–76
122. Czarnecki J. 2009. Stabilization of water in crude oil emulsions. Part 2. *Energy Fuels* 23:1253–57
123. Wu X. 2003. Investigating the stability mechanism of water–in–diluted bitumen emulsions through isolation and characterization of the stabilizing materials at the interface. *Energy Fuels* 17:179–90
124. Stanford LA, Rodgers RP, Marshall AG, Czarnecki J, Wu XA. 2007. Compositional characterization of bitumen/water emulsion films by negative- and positive-ion electrospray ionization and field desorption/ionization Fourier transform ion cyclotron resonance mass spectrometry. *Energy Fuels* 21:963–72
125. Buckley JS, Wang X, Creek JL. 2007. Solubility of the least-soluble asphaltenes. See Ref. 1, pp. 401–28
126. Buckley JS, Hirasaki GJ, Liu Y, Von Drasek S, Wang JX, Gill BS. 1998. Asphaltene precipitation and solvent properties of crude oils. *Pet. Sci. Technol.* 16:251–85
127. Hirschberg A, de Jong LNJ, Schipper BA, Meijer JG. 1984. Influence of temperature and pressure on asphaltene flocculation. *Soc. Pet. Eng. J.* 24:283–93
128. Maqbool T, Balgoa AT, Fogler HS. 2009. Revisiting asphaltene precipitation from crude oils: a case of neglected kinetic effects. *Energy Fuels* 23:3681–86
129. Ting PD, Gonzalez DL, Hirasaki GJ, Chapman WG. 2007. Application of the PC-SAFT equation of state to asphaltene phase behavior. See Ref. 1, pp. 301–24
130. Ting PD, Hirasaki GJ, Chapman WG. 2003. Modeling of asphaltene phase behavior with the SAFT equation of state. *Pet. Sci. Technol.* 21:647–61
131. Sirota EB, Lin MY. 2007. The physical behavior of asphaltenes. *Energy Fuels* 21:2809–15
132. Zhao B, Shaw JB. 2007. Composition and size distribution of coherent nanostructures in Athabasca bitumen and Maya crude oil. *Energy Fuels* 21:2795–804
133. Agrawala M. Yarranton HW. 2001. Asphaltene association model analogous to linear polymerization. *Ind. Eng. Chem. Res.* 40:4664–72

Annual Review of
Analytical Chemistry

Volume 4, 2011

Contents

Indexes

Errata

An online log of corrections to the *Annual Review of Analytical Chemistry* articles may be found at http://arjournals.annualreviews.org/errata/anchem